

Coarse Frame and Carrier Synchronization of OFDM Systems: A New Metric and Performance Evaluation

Kai Shi and Erchin Serpedin*

Abstract

This paper proposes a fast and reduced complexity frame and carrier acquisition scheme for orthogonal frequency division multiplex (OFDM) systems which assume either a continuous or a burst mode operation in additive white Gaussian noise (AWGN) and frequency-selective channels. By exploiting the repetitive structure of a training symbol, a robust frame synchronizer is obtained and shown to resume to finding the peak of a certain correlation metric that is obtained by invoking Maximum Likelihood principles. A new carrier estimator that can correct frequency offsets up to two subcarrier spacings is also proposed. The efficiency of the proposed synchronization algorithms is illustrated by both theoretical performance analysis and computer simulations.

Keywords

orthogonal frequency-division multiplexing (OFDM), maximum likelihood estimation, synchronization, training symbol

Kai Shi and Dr. Erchin Serpedin are with the Department of Electrical Engineering, Texas A&M University, College Station, TX 77843-3128, USA. Phone: (979) 458 2287, Fax: (979) 862 3128, email: serpedin@ee.tamu.edu.

*The corresponding author is Dr. Erchin Serpedin. This work was supported by the NSF Award No. CCR-0092901.

Permission to publish this abstract separately is granted

I. INTRODUCTION

Orthogonal frequency division multiplex (OFDM) systems have been adopted in many high bit rate wireless transmission systems such as DVB, HiperLAN and IEEE 802.11a. Due to the sensitivity of OFDM systems to synchronization errors, reliable synchronization schemes must be designed for these systems. By exploiting the known structure of a training symbol or a cyclic prefix, several schemes have been proposed for coarse estimation of the carrier frequency offset and timing delay [2]-[10], and [12].

In [3], the training symbol contains two identical halves [+A +A], and the timing delay estimator is obtained by searching for the peak of correlation between the first and second halves of the received symbols. By comparing the phase difference between the identical parts, a coarse frequency offset estimator is also proposed. However, the correlation peak of the timing metric exhibits a plateau which causes large variance for the timing estimator [5]. Based on a training preamble having the same structure as the one used in the Schmidl-Cox's estimator [3], reference [4] showed that the performance of the MMSE (Minimum Mean-Square Error) and ML (Maximum Likelihood) timing estimators still perform unsatisfactorily.

Similar to the signaling set-up adopted in [3], Coulson used two repeated m-sequences as a training symbol [8]-[9]. However, the proposed time synchronization algorithm is likely to fail in the presence of large carrier frequency offsets [11], and presents high implementation complexity due to the matched filtering. We remark also that a training symbol with the same structure as the one proposed in [8] is exploited in [10] to develop reliable frequency and time acquisition schemes. However, the proposed time synchronization algorithm is also sensitive to large frequency offsets [11].

By adopting a structured training symbol of the form [+B +B -B -B], Bhargava *et.al.* proposed a coarse timing delay estimator that outperformed Schmidl-Cox's estimator [5]. However, reference [5] does not provide any detailed insight or analysis pertaining to the features of this estimator. Inspired by the signaling set-up proposed in [5], this paper aims to develop reliable and reduced complexity coarse frame and carrier frequency acquisition schemes that exploit a structured training symbol of the form:

$$[\pm B \pm B \pm B \pm B], \quad (1)$$

where B stands for a sequence of $N/4$ training samples with constant variance (power) (e.g.,

an m-sequence), and it can be generated with good approximation by using an $N/4$ -point IFFT of an m-sequence. In fact, any signal with constant envelope in the time domain and a bandwidth similar to the OFDM data symbol can be used as a training symbol. It is found that among all the signaling set-ups (1), the training symbol:

$$[+B \ +B \ -B \ +B] , \quad (2)$$

leads to timing acquisition schemes that exhibit the best detection properties in terms of lower false detection probability and higher correct acquisition probability. In addition, it turns out that the negative term $-B$ present in (2) can be placed in any location with no loss in performance¹. By exploiting the structured training symbol (2), this paper proposes robust acquisition schemes for time delay and carrier frequency offset for OFDM systems that operate in additive white Gaussian noise (AWGN) and frequency-selective channels. The proposed time synchronizer offers more accurate estimates than the estimators [3] and [5]. It is also found that the performance of the proposed time and frequency offset estimators is nearly the same as [8]. In addition, the proposed estimator assumes a reduced implementation complexity and is more robust to large frequency offsets with respect to (w.r.t) [8].

The rest of paper is organized as follows. In Section II, we describe the signal model and introduce some modelling assumptions. In Section III, an optimum maximum likelihood (ML) estimator is derived for the continuous transmission scenario. We transform this ML estimator into a sub-optimum estimator that presents reduced complexity and exhibits robust performance to fading channel effects and large carrier frequency offsets for both burst and continuous transmission scenarios. A theoretical performance analysis study is conducted in Section IV. Finally, Section V describes computer simulations that illustrate the advantages of the proposed estimator and that corroborate the theoretical performance analysis performed in Section IV.

II. SIGNAL MODEL

The OFDM baseband signal is generated by the IFFT-transform:

$$x(n) = \frac{1}{\sqrt{N}} \sum_{k=0}^{N-1} s_k e^{j2\pi kn/N}, \quad -L \leq n \leq N-1, \quad (3)$$

¹All of them are similar to the Barker sequence of length 4.

where s_k represents the data sequence modulated on the k th subcarrier, which may assume any modulation format (such as QAM or PSK), and is independently and identically distributed (i.i.d.) with zero mean and variance $E\{|s_k|^2\} = \sigma_s^2$. Let N , L , and $1/T_u = 1/(NT_s)$ denote the number of subcarriers, the length of cyclic prefix (guard time), and the subcarrier spacing, respectively. Normally, the length of cyclic prefix L is selected to be not more than $N/5$, which can be interpreted as a 1-dB signal-to-noise ratio (SNR) loss introduced by the cyclic prefix [1, p. 46]. Herein, without loss of generality (w.l.o.g.) the value $L = N/8$ is adopted.

At the beginning of our study, we assume a flat fading channel model to derive the maximum likelihood estimator. Later it will be shown by computer simulations that the proposed estimator works well for frequency-selective channels, too. Assuming the sampling period $T_s = T_u/N$, the received signal samples can be expressed as:

$$r(n) = \alpha(n)x(n - \vartheta)e^{j(2\pi\varepsilon n/N + \theta)} + w(n), \quad (4)$$

where ϑ stands for the timing offset, $\alpha(n)$ is the channel amplitude, $\varepsilon := f_e T_u = f_e N T_s$ is the normalized carrier frequency offset, θ denotes the phase offset, and $w(n)$ denotes the samples of a zero-mean complex white Gaussian noise random process with variance $E\{|w(n)|^2\} = \sigma_w^2$ and is assumed independent w.r.t $x(n)$. In slow-varying channels, we can assume $\alpha(n)$ to be a constant α over the duration of several OFDM symbols. The signal-to-noise ratio is represented in terms of the variable $\text{SNR} := \alpha^2 \sigma_s^2 / \sigma_w^2$.

After coarse frame and carrier synchronization is achieved, the receiver discards the cyclic prefix, and the modulated symbol stream $\{s_k\}$ can be recovered by means of an FFT-operation. Due to the presence of cyclic prefix, small (fractional) time offsets ϑ in magnitude less than the interval (L) spanned by the cyclic prefix cause no ISI or interchannel interference (ICI) [12]-[13]. The time offset induces a phase offset $\exp(-j2\pi\vartheta n/N)$ on the n th subcarrier, which can be corrected using channel estimation techniques. Therefore, it is sufficient to estimate the start of the training sequence within one sample period.

This paper focuses on the estimation of ε and ϑ (packet detection). Although, α and θ are unknown to the receiver, their estimation can be avoided via differential encoding/decoding or can be obtained with channel estimation (pilot symbol based) techniques [12]-[13].

III. MAXIMUM LIKELIHOOD ESTIMATOR

To derive the maximum likelihood estimator, we use a method similar to the one reported in [7]. First, we consider the continuous transmission scenario. Assume that the length of the observation vector R is so long that it incorporates the whole training symbol $[r(d) \cdots r(d+N-1)]^T$:

$$R := [r(d-p) \quad r(d-p+1) \cdots r(d) \cdots r(d+N-1) \quad r(d+N) \cdots r(d+N+q-1)]^T, \quad (5)$$

where $U := p + q + N$ denotes the length of the observation vector R , p and q stand for the lengths of the subvectors preceding and succeeding the training symbol, respectively. Due to the repetitive structure of the training symbol, the autocorrelation function of the observation vector takes the form:

$$\Phi_{rr}(m) := E\{r(n)r^*(n+m)\} = \begin{cases} \alpha^2\sigma_s^2 + \sigma_w^2, & m = 0 \\ (-1)^{t+1}\alpha^2\sigma_s^2\beta^t, & m = tN/4; n \in \Gamma_1; t = 1, 2, 3 \\ (-1)^t\alpha^2\sigma_s^2\beta^t, & m = tN/4; n \in \Gamma_2; t = 1, 2 \\ -\alpha^2\sigma_s^2\beta, & m = N/4; n \in \Gamma_3 \\ 0, & \text{otherwise,} \end{cases} \quad (6)$$

where α is assumed to be constant during the whole observation vector R , $\beta := \exp(-j\pi\varepsilon/2)$ and $\Gamma_i := [r_{d+(i-1)N/4} \cdots r_{d+iN/4-1}]^T$, $i = 1, \dots, 4$, represents the received samples corresponding to the i th part of the training symbol.

For the channel assumed in (4), we obtain the conditional probability density function (pdf) of the observation vector R w.r.t. $\{d, \varepsilon\}$ in the form

$$f(R | \varepsilon, d) = \frac{\exp(-R^H C^{-1} R)}{(2\pi)^U \det(C)}, \quad (7)$$

where $[\cdot]^H$ is the hermitian transposition operator and C is the autocorrelation matrix of the observation vector R . Let I_k stand for the identity matrix of dimension k . From (6), it follows that

$$C = \text{diag}\{\Phi_{rr}(0)I_p, \quad H_N, \quad \Phi_{rr}(0)I_q\}, \quad (8)$$

where H_N is the block hermitian matrix

$$H_N := (\alpha^2 \sigma_s^2 + \sigma_w^2) \begin{pmatrix} 1 & \rho\beta & -\rho\beta^2 & \rho\beta^3 \\ \rho\beta^{-1} & 1 & -\rho\beta & \rho\beta^2 \\ -\rho\beta^{-2} & -\rho\beta^{-1} & 1 & -\rho\beta \\ \rho\beta^{-3} & \rho\beta^{-2} & -\rho\beta^{-1} & 1 \end{pmatrix} \otimes I_{N/4}, \quad (9)$$

where $\rho := \text{SNR}/(\text{SNR} + 1)$ and \otimes denotes the Kronecker product. Since C has a diagonal structure, its inverse is still diagonal:

$$C^{-1} = \text{diag}\{(1/\Phi_{rr}(0))I_p, \quad H_N^{-1}, \quad (1/\Phi_{rr}(0))I_q\}. \quad (10)$$

Exploiting the hermitian symmetry of H_N and the following property of the Kronecker product $(A \otimes B)^{-1} = A^{-1} \otimes B^{-1}$, some calculations show that:

$$H_N^{-1} = \kappa \begin{pmatrix} 2\rho + 1 & -\rho\beta & \rho\beta^2 & -\rho\beta^3 \\ -\rho\beta^{-1} & 2\rho + 1 & \rho\beta & -\rho\beta^2 \\ \rho\beta^{-2} & \rho\beta^{-1} & 2\rho + 1 & \rho\beta \\ -\rho\beta^{-3} & -\rho\beta^{-2} & \rho\beta^{-1} & 2\rho + 1 \end{pmatrix} \otimes I_{N/4}, \quad (11)$$

where $\kappa := 1/(1 + 2\rho - 3\rho^2)$. Substituting (10) and (11) into (7), after some lengthy algebraic manipulations, the pdf of R w.r.t. $\{\varepsilon, d\}$ becomes

$$\begin{aligned} f(R | \varepsilon, d) &= \frac{1}{(2\pi)^U \det(C)} \\ &\exp \left\{ \frac{-1}{(\alpha^2 \sigma_s^2 + \sigma_w^2)} \left[\sum_{n=d-p}^{d+N+q-1} |r(n)|^2 + 3\rho\kappa \sum_{n=d}^{d+N-1} |r(n)|^2 + 2\kappa \Re \left(\sum_{n=d}^{d+N/4-1} \right. \right. \right. \\ &[-r^*(n)r(n + N/4) + r^*(n + N/4)r(n + N/2) + r^*(n + N/2)r(n + 3N/4)]\beta \\ &\left. \left. \left. + [r^*(n)r(n + N/2) - r^*(n + N/4)r(n + 3N/4)]\beta^2 - r^*(n)r(n + 3N/4)\beta^3 \right] \right\}, \quad (12) \end{aligned}$$

where $\det(C)$ is a constant that does not depend on ε and d .

The maximum likelihood estimator for the time and carrier frequency offset is given by

$$(\hat{\varepsilon}, \hat{d}) = \arg \max_{\bar{\varepsilon}, \bar{d}} f(R | \bar{\varepsilon}, \bar{d}), \quad (13)$$

where $\bar{\varepsilon}$ and \bar{d} stand for the trial values corresponding to time and frequency offset, respectively. Defining sub-vectors $R_i := [r(\bar{d} + (i - 1)N/4), \dots, r(\bar{d} + iN/4 - 1)]^T$, $i = 1, \dots, 4$,

and omitting the constants which are independent of ε and d , we obtain the log-likelihood function:

$$\begin{aligned}
\Lambda(\bar{\varepsilon}, \bar{d}) &= 3\rho \sum_{i=1}^4 |R_i|^2 - 2\Re\mathbf{e}[\underbrace{(R_1^H R_2 - R_2^H R_3 - R_3^H R_4)}_{P_1(\bar{d})}\beta + \underbrace{(R_2^H R_4 - R_1^H R_3)}_{P_2(\bar{d})}\beta^2 + \underbrace{R_1^H R_4}_{P_3(\bar{d})}\beta^3] \\
&\geq 3\rho \sum_{i=1}^4 |R_i|^2 - 2\Re\mathbf{e}[|P_1(\bar{d})\beta| + |P_2(\bar{d})\beta^2| + |P_3(\bar{d})\beta^3|] \\
&= 3\rho \sum_{i=1}^4 |R_i|^2 - 2\underbrace{[|P_1(\bar{d})| + |P_2(\bar{d})| + |P_3(\bar{d})|]}_{P(\bar{d})}, \tag{14}
\end{aligned}$$

where $|R_i|^2 := R_i^H R_i$. The expression (14) represents a decoupled timing metric $\Lambda(\bar{d})$ which still depends on the unknown time-varying amplitude α . We observe also that the first term of $\Lambda(\bar{d})$ is a power estimate of R . If we divide $\Lambda(\bar{d})$ by its first term and omit the unknown factor ρ , the following normalized time metric results:

$$Q(\bar{d}) := \frac{P(\bar{d})}{\frac{3}{2} \sum_{i=1}^4 |R_i|^2}. \tag{15}$$

Later we will show that the mean value of $Q(\bar{d})$ is independent of α in quasi-static channels. Hence, we have obtained a decoupled implementation of the time and frequency offset estimators for flat fading channels:

$$\hat{d} := \arg \max_{\bar{d}} Q(\bar{d}), \tag{16}$$

$$\hat{\varepsilon} := \frac{2}{\pi} \arg P_1(\hat{d}). \tag{17}$$

Let us consider the burst transmission scenario, e.g., a time division duplex (TDD) system. Normally, the received frame is preceded by noise only. The autocorrelation matrix C is block diagonal:

$$C = \text{diag}\{\sigma_w^2 I_p, \quad H_N, \quad (\alpha^2 \sigma_s^2 + \sigma_w^2) I_q\}. \tag{18}$$

Using techniques similar to the ones depicted previously, we can obtain a log-likelihood function which incorporates the dependency on the unknown number (p) of noise-like terms preceding the training symbol in the observation vector R . Fortunately, as shown in Fig. 1, the timing metric (15) still achieves a maximum value at the start of the frame. Therefore, (16) and (17) can be used in both continuous and burst transmission scenarios. Since the proposed

training symbol based fast acquisition scheme is more fit for burst mode transmissions, the following analysis will focus on burst transmission scenarios.

Defining $l := \bar{d} - d$, after some lengthy algebraic manipulations (see Appendix-A), at high SNR, we can approximate $P(l)$ as a real non-central Gaussian random variable (RV) with mean and variance

$$\mu_P := (3N/2 - 7|l|)\sigma_s^2\alpha^2, \quad \sigma_P^2 := (9N - 31|l|)\sigma_s^2\sigma_w^2\alpha^2/2, \quad (19)$$

respectively, and which represent good approximations in the range $|l| \leq N/6$. By replacing² the denominator of (15) by $V(l) = \frac{3}{2} \sum_{i=3}^4 |R_i|^2$, the following metric is obtained:

$$Q(l) = \frac{P(l)}{\frac{3}{2} \sum_{i=3}^4 |R_i|^2}. \quad (20)$$

Note also that $V(l)$ can be approximated for $|l| \leq N/2$ as a real Gaussian RV with mean and variance (see Appendix-A)

$$\mu_V := 3N/2(\sigma_s^2\alpha^2 + \sigma_w^2), \quad \sigma_V^2 := 9N\sigma_w^2(\sigma_s^2\alpha^2 + \sigma_w^2/2). \quad (21)$$

Thus, $V(l)$ is independent of l when $|l| \leq N/2$. Substituting (19) and (21) into (20), the mean of $Q(l)$ can be evaluated

$$\mu_Q := \left(1 - \frac{14|l|}{3N}\right) \cdot \rho \approx 1 - \frac{14|l|}{3N} \quad (\text{high SNR}), \quad (22)$$

which is independent of α at high SNR in quasi-static flat fading channels.

For the training symbol [+A +A], a timing metric similar to (20) is proposed in [8]

$$Q'(l) = \frac{P'(l)}{V'(l)} = \frac{|R_1^H R_2 + R_3^H R_4|}{|R_1|^2 + |R_2|^2}, \quad (23)$$

and its mean value is given by $\mu'_Q = (1 - 2|l|/N)\rho$.

Fig. 1-a depicts the expected value of the time metrics corresponding to two different OFDM signaling set-ups with 128 subcarriers each. The plots illustrate that the experimental value of the mean of metric $Q(l)$ is very close to the theoretical value (22) for $-N/6 \leq l < 0$. Actually, the approximation (22) holds only for $-N/6 \leq l < 0$ (see Appendix-A). However,

²One explanation for this modification is that we try to keep μ_Q as small as possible for $|l| < N/2$ to obtain robust packet detection.

a similar analysis can be made for $l < -N/6$, as it is shown by the experimental values depicted in Fig. 1-a. A slightly increased discrepancy between the theoretical values (22) and the experimental values appears whenever $l > 0$, a result which is due to the fact that the samples succeeding the training symbol contain data besides noise. Fig. 1-a shows that the timing metric corresponding to the training symbol [+B +B -B +B] has a much better localization property than that corresponding to the training symbol [+A +A]. Later on, simulation experiments will be presented to illustrate further that the proposed time acquisition scheme is robust to both ISI effects and carrier frequency offsets.

In [5], Bhargava *et al.* proposed a slightly different training symbol [+B +B -B -B]. Using the same method as before, the timing metric corresponding to the training symbol [+B +B -B -B] takes the expression:

$$Q_1(l) = \frac{|R_1^H R_2 + R_3^H R_4 - R_2^H R_3| + |R_1^H R_3 + R_2^H R_4| + |R_1^H R_4|}{3(|R_3|^2 + |R_4|^2)}. \quad (24)$$

By performing a similar analysis, the mean value of $Q_1(l)$ can be evaluated. In Fig. 1-b, the mean values of several timing metrics are plotted. When compared with the timing metric (20) corresponding to the training symbol [+B +B -B +B], the timing metric (24) has two undesirable peaks located in both intervals of the region $|l| > N/6$. In [5], Bhargava proposed a timing metric similar to (24)

$$Q_2(l) = \frac{|R_1^H R_2 + R_3^H R_4|}{0.5(\sum_{i=1}^4 |R_i|^2)}, \quad (25)$$

which is found to present a large undesirable correlation peak as shown in Fig. 1-b, and consequently appears not to be appropriate for burst transmission scenarios. If only the last two terms in the denominator of (25) are considered, the following modified timing metric is obtained:

$$Q_3(l) = \frac{|R_1^H R_2 + R_3^H R_4|}{|R_3|^2 + |R_4|^2}. \quad (26)$$

Fig. 1-b shows that the modified timing metric $Q_3(l)$ has four undesirable local peaks besides the desired correlation peak. Thus, the modified metric is less reliable than (24). Since the timing metrics (24)-(26) have some undesirable peaks besides the desired correlation peak, in what follows we will focus our analysis on the timing metric (20) corresponding to the proposed training symbol (2).

The implementation of the timing acquisition scheme requires searching techniques for finding the correlation peak of the timing metric. In [9], Coulson proposed a two-step based searching technique for packet detection. We adapted this two-step searching technique to fit the proposed timing metric.

Step 1: Coarse packet detection. A detection threshold T_c is set up to assure that the receiver can find the peak of the metric in a short range. The estimator compares $Q(l)$ with a given threshold T_c . Once $Q(l) > T_c$, the receiver obtains a coarse packet detection range Ω and proceeds with the next step.

Step 2: Fine packet detection and frequency offset estimation. In this step, the receiver searches for the local peak³ of $P(l)$ in the range Ω , and the frequency offset estimator is implemented using (17). The resolution of this search step is limited to one sampling period.

Normally, the coarse estimated value l obtained in the first step is always negative (we assume w.l.o.g. that $|l| \leq \Omega$), a fact which will be corroborated in the next section (see Fig. 3). To detect the correct start ($l = 0$) of the packet, the receiver needs to search the maximum of $P(l)$ by sliding the observation window R in a continuous interval that runs from l to $l + \Omega$ and that contains the correct starting point ($l = 0$) of the frame. Figs. 2-a and 2-b depict two critical scenarios, where the right acquisition time is present at one of the extremities of the searching interval. In any case, the receiver requires a processing delay in the second step, which depends on the value Ω . Thanks to the guard time (cyclic prefix) of the succeeding OFDM symbol, as shown in the Fig. 2, if $\Omega = L$, then the correct correlation peak can be found in a search range equal to L . Fig. 2-b shows that the last location of the sliding window will not overlap with the useful part of the succeeding OFDM symbol. Thus, the second step requires a processing delay not larger than L .

Based on the above considerations, in the first step the following condition must be satisfied for the success of fine packet detection step

$$\text{for any } l < -L, \quad Q(l) < T_c, \quad \text{and there exists } l \in [-L, 0] \text{ such that } Q(l) > T_c, \quad (27)$$

which means that the coarse packet detection is obtained only in the range of $[-L + 1, 0]$.

³ $Q(l)$ can also be used in this step and we have found out that the searches based on these two different metrics have almost the same performance in slow-varying channels. We consider the metric $P(l)$ to simplify the analysis.

IV. THEORETICAL ANALYSIS OF ESTIMATORS

In this section we perform a theoretical analysis of the estimators proposed in the previous section. Since most of the detected peaks are delayed several samples from the correct time in multipath environments (see Fig. 8) and OFDM is tolerant to this kind of errors whenever a short cyclic postfix is present, in what follows we will limit the analysis of estimators only for lags $l \leq 0$. Since the samples succeeding the training symbol contain data besides noise, we remark that the analysis is right only for $l \leq 0$. The analysis for $l > 0$ appears intractable.

A. Coarse Packet Detection

We use the same method as in [9], and define:

$$Z(l) := P(l) - T_c V(l) \quad . \quad (28)$$

The receiver will declare it obtains coarse packet detection once $Z(l) > 0$. Since both $P(l)$ and $V(l)$ can be approximated as real Gaussian RVs for high SNR, it follows that

$$p_{1r} := \text{prob}(Z(l) > 0) = \frac{1}{2} \text{erfc} \left(-\frac{\mu_Z}{\sqrt{2}\sigma_Z} \right) \quad , \quad (29)$$

where

$$\mu_Z := \mu_P - T_c \mu_V \quad , \quad \sigma_Z^2 := \sigma_P^2 + T_c^2 \sigma_V^2 - 2T_c \text{cov}\{P, V\} \quad . \quad (30)$$

From Fig. 3 we infer that (27) can be satisfied with probability asymptotically approaching 1.0 when $T_c = 0.6$ and $\text{SNR} > 10$ dB. As for $[+A \ +A]$, there is no threshold value to get robust (high probability) coarse packet detection in the range $-L \leq l \leq 0$. A longer cyclic prefix length L , e.g., $L = N/4$, can increase the probability of coarse packet detection, but at the same time the system throughput is reduced.

In the absence of signal, the product of two noise vectors can not be omitted like the approximation performed in Appendix-A. From [8], according to the Central Limit Theorem (CLT), $P_1(l)$, $P_2(l)$ and $P_3(l)$ can be approximated as three Gaussian RVs with variances $\sigma_i^2 := (1 - i/4)N\sigma_w^4$, $i = 1, 2, 3$, respectively. From (14), $P(l)$ can be viewed as the summation of three independent Rayleigh RVs with the pdfs $f(x_i) = 2x_i/\sigma_i^2 \exp(-x_i^2/\sigma_i^2)$, $i = 1, 2, 3$.

Note also that $V(l)$ can be viewed as a Gaussian RV with mean $\mu_V := 3N\sigma_w^2/2$ and variance $\sigma_V^2 := 9N\sigma_w^4/2$. Since a closed-form expression for the probability of false alarm

$p_{FA} := \text{prob} (|P_1(l)| + |P_2(l)| + |P_3(l)| > T_c V(l))$ can not be obtained, we resorted to numerical calculations. For $N = 128$ and $T_c = 0.6$, an extremely small value is obtained $p_{FA} = 1.38e - 9$. Increasing the threshold T_c and training symbol length N can reduce further the probability of false alarm (see Fig. 4). It is interesting to note that an upper bound of p_{FA} may be obtained based on the inequality $p_{FA} < \text{prob} (3|P_1(l)| > T_c V(l)) \approx \exp(-NT_c^2/(3 + 4T_c^2))/\sqrt{1 + 4T_c^2/3}$, which shows an exponential dependence w.r.t. N .

B. Fine Packet Detection

First, we derive the probability of a type of estimation error that takes place at the closest neighbor to the correct time location. In Appendix-B, it is shown that $\Delta := P(0) - P(-1)$ can be viewed as a real Gaussian RV with mean $\mu_\Delta = 7\sigma_s^2\alpha^2$ and variance $\sigma_\Delta^2 := (41 + 12\cos(\beta))\sigma_s^2\sigma_w^2\alpha^2 < 53\sigma_s^2\sigma_w^2\alpha^2$. The probability of $\Delta < 0$ can be expressed as

$$p_{2r} := \text{prob}\{\Delta < 0\} = \frac{1}{2}\text{erfc}\left(\frac{\mu_\Delta}{\sqrt{2}\sigma_\Delta}\right) < \frac{1}{2}\text{erfc}\left(7\sqrt{\frac{\text{SNR}}{106}}\right). \quad (31)$$

At high SNR, p_{2r} is very small, e.g., $p_{2r} < 0.0033$, at SNR= 9 dB. Thus, the detected correlation peak deviates from the correct location to the closest neighbor with small probability. Similarly, the probabilities of $P(l) > P(0)$ for $-\Omega \leq l < -1$ ($\Omega = L = N/8$) can be determined based on some similar calculations and they are much smaller than p_{2r} . Thus, we can approximate the probability of fine packet detection p_{fd} by $p_{fd} \approx 1 - p_{2r}$.

As for the training symbol [+A +A], if the timing metric $P'(l)$ (see (23)) is defined, a similar result can be obtained for the difference between the time metric corresponding to the correct time and that corresponding to its closest neighbor, $\Delta' = P'(0) - P'(-1)$. In Fig. 5, it is shown that the normalized (with the same mean) variance of Δ' is much larger than the normalized variance of Δ . Define

$$p_{3r} := \text{prob}\{\Delta' < 0\} = \frac{1}{2}\text{erfc}\left(\sqrt{\frac{\text{SNR}}{6}}\right). \quad (32)$$

It follows that a higher probability for detecting a (false) peak deviating from the correct time to its neighborhood is expected for the Schmidl-Cox's estimator [3], (e.g., $p_{3r} = 0.05$ when SNR= 9dB). The above analysis shows that the proposed timing metric is more robust than the timing metric corresponding to the training symbol [+A +A].

C. Carrier Frequency Offset Estimation

According to (17), the identifiability limit of the proposed carrier frequency offset estimator is given by $|\varepsilon| < 2$, which is equal to twice the subcarrier spacing and is larger than that corresponding to estimators [2], [3] and [8]. If there is no timing error, the estimator (17) is shown (in Appendix-C) to be an unbiased estimator with mean-square error:

$$\text{MSE}[\hat{\varepsilon}] \approx \frac{16}{9 \cdot \pi^2 \cdot N \cdot \text{SNR}}, \quad (33)$$

which is even smaller than the MSE of the frequency offset estimator proposed in [3]. In the presence of small timing errors $l \neq 0$ this estimator is shown (see Appendix-C) to be still unbiased and its mean-square error is given by:

$$E[(\hat{\varepsilon} - \varepsilon)^2] \approx \frac{16 \cdot (1 + \frac{10|l|}{N})}{9 \cdot \pi^2 \cdot N \cdot \text{SNR} \cdot (1 - \frac{4|l|}{N})^2}. \quad (34)$$

The MSE of the frequency offset estimator depends on the timing error, SNR and the length of training symbol. Fig. 6-b indicates that small timing offsets result in little degradation.

Assume now the following general form of a training symbol with length N

$$[b_1 S_1^T \ b_2 S_2^T \ \cdots \ b_M S_M^T]^T, \quad (35)$$

where $S_i = B$, $i = 1, \dots, M$, are identical sub-vectors of length N/M , and $b_i = \pm 1$ represents a bit sign (\pm) associated with S_i . We observe that the signaling set-ups proposed in [3], [8], and in this paper are special cases of (35) $M = 2$, $b_1 = b_2 = 1$, and $M = 4$, $b_1 = b_2 = b_4 = 1$, $b_3 = -1$, respectively.

If R_i is the observation vector corresponding to $b_i S_i$ corrupted by the AWGN vector W_i , a general estimator for ε can be expressed as:

$$\hat{\varepsilon} = \frac{M}{2\pi} \arg \left(\frac{\Im[\sum_{i=1}^{M-1} b_i b_{i+1} R_i^H R_{i+1}]}{\Re[\sum_{i=1}^{M-1} b_i b_{i+1} R_i^H R_{i+1}]} \right), \quad (36)$$

which is unbiased, and the following general expression for the MSE of the frequency estimator holds (see Appendix C):

$$\text{MSE}[\hat{\varepsilon}] = \frac{M^3}{4 \cdot \pi^2 \cdot (M-1)^2 \cdot N \cdot \text{SNR}}. \quad (37)$$

For a fixed SNR and N , the value $M = 4$ minimizes (37) within the set of all even integers. This result is corroborated by the set of curves depicted in Fig. 6-a. When compared with [3] and [8], the proposed estimator (17) achieves a similar MSE-performance but assumes a larger (twice) estimation range.

In [8], Coulson used the same coarse correlator as [3] before the matched filter to estimate and correct the fractional frequency offset $|\varepsilon| < 1$. Unfortunately, the received samples after Coulson's coarse frequency estimator might still be affected by large frequency offsets $|\varepsilon| > 1$, which will cause the failure of the fine packet detection step [11]. However, we note that the proposed frequency estimator (17) is robust to large frequency offsets.

It is interesting that this single sliding window estimator (SSE) in (36) is a sub-optimal and the simplest version of estimators used in [14] and [15]. References [14] and [15] propose the best linear unbiased estimator (BLUE), which achieves the minimal variance by increasing the complexity ($M/2$ sliding windows and properly weighted averaging). In Fig. 7, we compare the performance and complexity between SSE and BLUE for different values of the parameter M , which determines the frequency offset detection range. The designer can choose a tradeoff between performance, detection range and complexity. Constrained by the performance requirement (e.g., MSE less than 10^{-4}), we should use the BLUE estimator to detect large frequency offsets. If only small frequency offsets are to be compensated, the reduced complexity SSE estimator can be selected.

Different from the above estimators, a nonlinear least-squares (NLS) approach was proposed in [16]. An accurate NLS frequency offset estimation can be obtained by using large FFT search grids, which lead to an increased complexity estimator.

V. NUMERICAL ANALYSIS OF ESTIMATORS

We assume a wireless OFDM system of bandwidth 5 MHz operating at 5.8 GHz, with $N = 128$ subcarriers and cyclic prefix $L = 16$. The channel is time-varying continuously with a maximum Doppler frequency of 50 Hz and has an exponentially decaying power-delay profile with 16 independent T_s -spaced Rayleigh-fading paths that are modelled in accordance with Jakes model. The root-mean square delay spread for this power-delay profile is assumed $\tau_{rms} = 1$ sample, and the maximum delay spread is 16 samples. A frequency offset $f_e = 0.8NT_s$ is assumed. A number of 2,000 Monte Carlo trials were performed for each SNR

point.

A. The Performance of Algorithms

The performance of five algorithms are compared by computer simulation: (a) Schmidl-Cox method [3], (b) Modified method A, which assumes the timing metric $Q'(l)$ (23) and the training symbol [+A +A] (no cyclic prefix), (c) Modified method B, which assumes the timing metric (26), (d) Proposed method (20), and (e) Coulson's method [8]. We assume that methods (a)-(d) use the same searching techniques as the ones proposed in Section III. The threshold value for the coarse packet detection step is set to $T_c = 0.6$ for all five methods and $\text{SNR} \geq 6$ dB. The second threshold value for the matched filter in [8] is set to 0.5. Because of the poor localization properties of the Schmidl-Cox method and the modified method A, we extend the searching range from L to $2L$ during the second searching step.

At $\text{SNR}=20$ dB, the distributions of timing estimation errors l are shown in Figs. 8, where the path with strongest power is assumed to be the correct time. The high inaccuracy of the Schmidl-Cox method (in Fig. 8-a) is due to the cyclic prefix which causes a plateau for the timing metric [5]. In Figs. 8 b-e, most estimation errors are delayed values in the range $0 \leq l \leq 2$. The delayed errors will result in interference between adjacent symbols. In [17], a short cyclic postfix is used to mitigate ISI errors due to delayed FFT windows. Here we use a cyclic postfix with length 2 for the OFDM symbols succeeding the training symbol.

The timing errors $l > 2$ or $l < 0$ will still cause ISI, and we compare the probabilities of this kind of timing errors for all the five estimators in Fig. 9. Most timing errors of the Schmidl-Cox method induce ISI and a longer cyclic prefix for succeeding symbols is needed to decrease the ISI, which means a loss in the system throughput. Although no cyclic prefix (no plateau for timing metric) is used in the modified method A, its performance is worse than methods (c) and (d). The performance of method (c) is close to that of the proposed estimator. But in our simulation, we use high quantization resolution (limited by computer) when calculating the timing metrics. If a small quantization resolution (e.g., 6 bits) is used, due to its undesirable peaks beside the correct peak in Fig. 2, it can be expected that the packet detection of method (c) is much worse than that of the proposed scheme. Due to the excellent autocorrelation characteristic of m-sequences, it is not surprising that Coulson's method provides the best performance. However, Coulson's method is sensitive to large

frequency offsets as discussed in [11].

Next, we compare the performance of frequency offset estimators. The same frequency offset estimator as [3] is used in the case of estimators (a) and (b). No carrier estimator was proposed in [5]. Therefore, we extend the corresponding frequency estimator here. Since (26) exploits only the set of statistics $R_1^H R_2$ and $R_3^H R_4$, a frequency offset estimator similar to (17) and which exploits only the reduced set of statistics present in (26) can be expressed as:

$$\hat{\varepsilon} := \frac{2}{\pi} \arg(R_1^H R_2 + R_3^H R_4) . \quad (38)$$

From Fig. 10, it is concluded that the MSE of the proposed estimator is almost the same as that of Coulson method and modified method A. However, the proposed estimator (17) exhibits a larger identifiability range. The larger MSE of (38) is due to the neglected statistics $R_2^H R_3$. Thanks to the cyclic prefix, which preserves the periodic correlation among the samples of the received signal in the presence of slow varying multipath channel, the Schmidl-Cox frequency estimator provides better performance than the other methods, especially at high SNR. According to [1], for a negligible degradation of about 0.1 dB, the maximum tolerable frequency offset is less than 1% of the subcarrier spacing, a condition which is satisfied by all estimators (excluding the estimator (38)) whenever $\text{SNR} > 13\text{dB}$. Therefore, we expect that this improvement of the frequency offset estimate due to the cyclic prefix present in the training symbol can hardly improve the BER performance. Actually, the BER performance will degrade due to the large timing errors created by the presence of the cyclic prefix (see Fig. 8-a), a fact that will be later verified by simulations.

B. System Performance

In order to assess the performance of the proposed synchronization scheme, we compare the BER performance of three systems: the proposed scheme (dash line), the Schmidl-Cox scheme (dash-dot line), and the perfect synchronization scenario (solid line), respectively. We use DQPSK/DBPSK modulations in the frequency domain to simplify the receiver. An 1/2-rate convolutional code with 16 states, and block interleaving are utilized to correct random and burst errors caused by additive noise and frequency nulls created by deep fades.

When compared to the system with ideal synchronization, the Schmidl-Cox scheme presents a large degradation for both DBPSK and DQPSK modulations (see Fig. 11). As shown in

the Fig. 8-a, the detected value l often deviates from the start of the frame ($l = 0$) in the presence of dispersive channels. The timing errors have two impacts and both of them degrade the BER. First, a phase rotation $\exp(j2\pi ln/N)$ is induced by small timing errors $l \leq 2$, which leads to a constant phase difference $\exp(j2\pi l/N)$ between the adjacent subcarriers. The second impact and main reason for degradation is ISI induced by timing errors $l > 2$.

As for the system with the proposed scheme (dash line), for DBPSK, it has almost the same performance as the system with ideal synchronization. However, for DQPSK, the proposed estimator results in 0.3-dB degradation. The main reason for this degradation is due to the phase rotation induced by small timing errors $l \leq 2$. However, this degradation can almost always be avoided by using channel estimation techniques to correct the linear phase offset between adjacent subcarriers.

VI. CONCLUSIONS

Motivated by the need to obtain a clear assessment of Barghava's estimator [5], this paper developed a fast and robust frame and carrier synchronization scheme for burst and continuous-mode OFDM transmissions in AWGN and ISI-channels. The proposed scheme exploits the repetitive structure of a training symbol and presents superior performance w.r.t. the Schmidl-Cox approach [3] and Bhargava's method [5] in terms of better detection properties and accuracy, and extended identifiability range of the carrier estimate. When compared with Coulson's method [8], the proposed scheme presents a reduced implementation complexity⁴, and is more robust to large carrier offsets and exhibits nearly the same performance in terms of estimation accuracy. It is also interesting to remark that the structure of the proposed training sequence can be expressed directly in terms of a length-4 Barker sequence.

Appendix A: Statistical Properties of Correlator Output at High SNR

Assuming a small time offset $l < 0$ from the start of frame, the observation vector R around the location of the training symbol can be expressed as

$$R = \alpha X e^{j(2\pi \varepsilon n/N + \theta)} + W, \quad (39)$$

⁴For each sample, the proposed scheme needs 8 complex products while Coulson's method needs $N/2+4$ complex products.

where $X := [X_1^T \ X_2^T \ X_3^T \ X_4^T]^T$ is the observed training symbol shifted by l samples from the correct time and $W := [W_1^T \ W_2^T \ W_3^T \ W_4^T]^T$ is the white noise vector independent w.r.t. X .

Let S_1 and S_2 denote the first and the second part of $S (= B)$ with lengths $N/4 - |l|$ and $|l|$, respectively. Thus, it is easy to rewrite $X_1 = \underbrace{[0 \ \cdots \ 0]}_{|l|} S_1^T]^T$, $X_2 = [S_2^T \ S_1^T]^T$, $X_3 = [S_2^T \ -S_1^T]^T$ and $X_4 = [-S_2^T \ S_1^T]^T$. Let W_{i1} and W_{i2} , $i = 1, 2, 3, 4$, represent the first and the second part of W_i with lengths $|l|$ and $N/4 - |l|$, respectively. The following relations hold

$$\begin{aligned}
P_1(l) &= R_1^H R_2 - R_2^H R_3 - R_3^H R_4 \\
&= \beta^{-1} \{ (3N/4 - 3|l|) \sigma_s^2 \alpha^2 + \alpha [W_{11}^H S_2 + W_{12}^H S_1 - W_{21}^H S_2 \beta^{-1} + 2\Re(S_1^H W_{22} \beta - S_1^H W_{32} \beta^2) \\
&\quad - 2\Im(S_2^H W_{31} \beta^2) + S_1^H W_{42} \beta^3 - S_2^H W_{41} \beta^3] \} + W_1^H W_2 - W_2^H W_3 - W_3^H W_4 \\
&\approx \beta^{-1} \{ (3N/4 - 3|l|) \sigma_s^2 \alpha^2 + \alpha [W_{11}^H S_2 + W_{12}^H S_1 - W_{21}^H S_2 \beta^{-1} + 2\Re(S_1^H W_{22} \beta - S_1^H W_{32} \beta^2) \\
&\quad - 2\Im(S_2^H W_{31} \beta^2) + S_1^H W_{42} \beta^3 - S_2^H W_{41} \beta^3] \}, \tag{40}
\end{aligned}$$

where we omit the products of two noise vectors. Thus, $P_1(l)$ can be approximated by a complex Gaussian RV. As for $|P_1(l)| := \sqrt{\Re^2(P_1(l)) + \Im^2(P_1(l))}$, it is a Rice RV. At high SNR, it is accurate to approximate $|P_1(l)|$ by its real part

$$\begin{aligned}
|P_1(l)| &\approx \Re(P_1(l)) = (3N/4 - 3|l|) \sigma_s^2 \alpha^2 + \alpha \Re [W_{11}^H S_2 + W_{12}^H S_1 - W_{21}^H S_2 \beta^{-1} \\
&\quad + 2W_{22}^H S_1 \beta^{-1} - 2W_{32}^H S_1 \beta^{-2} + W_{42}^H S_1 \beta^{-3} - W_{41}^H S_2 \beta^{-3}], \tag{41}
\end{aligned}$$

which is correct for $-N/4 \leq l \leq 0$ to keep the first term (signal part) positive. Similarly, for $-N/6 \leq l \leq 0$, we can approximate $|P_2(l)|$ by

$$\begin{aligned}
|P_2(l)| &\approx (N/2 - 3|l|) \sigma_s^2 \alpha^2 + \alpha \Re (-W_{11}^H S_2 + W_{12}^H S_1 - W_{21}^H S_2 \beta^{-1} \\
&\quad + W_{22}^H S_1 \beta^{-1} - W_{32}^H S_1 \beta^{-2} + W_{41}^H S_2 \beta^{-3} + W_{42}^H S_1 \beta^{-3}). \tag{42}
\end{aligned}$$

For $-N/4 \leq l \leq 0$, $|P_3(l)|$ can also be approximated as

$$|P_3(l)| \approx (N/4 - |l|) \sigma_s^2 \alpha^2 + \alpha \Re (-W_{11}^H S_2 + W_{12}^H S_1 + W_{42}^H S_1 \beta^{-3}). \tag{43}$$

Based on (41)-(43), for $-N/6 \leq l \leq 0$, it follows that

$$\begin{aligned}
P(l) &\approx (3N/2 - 7|l|) \sigma_s^2 \alpha^2 + \alpha \Re (-W_{11}^H S_2 + 3W_{12}^H S_1 - 2W_{21}^H S_2 \beta^{-1} \\
&\quad + 3W_{22}^H S_1 \beta^{-1} - 3W_{32}^H S_1 \beta^{-2} + 3W_{42}^H S_1 \beta^{-3}), \tag{44}
\end{aligned}$$

which is made up of a number of real Gaussian random variables. Thus, $P(l)$ can be viewed as a real Gaussian RV. As for $V(l)$, we approximate it by

$$V(l) = 3(N - |l|)\sigma_s^2\alpha^2/2 + 6\alpha\Re\mathbf{e}(W_{31}^H S_2 - W_{41}^H S_2 - W_{32}^H S_1 + W_{42}^H S_1) + 3|W_3|^2 + 3|W_4|^2. \quad (45)$$

From [8], if $N/2$ is sufficiently large, according to the CLT, $V(l)$ can be approximated as a real Gaussian RV with mean and variance:

$$\mu_V := 3N/2(\sigma_s^2\alpha^2 + \sigma_w^2), \quad \sigma_V^2 := 9N\sigma_w^2(\sigma_s^2\alpha^2 + \sigma_w^2/2), \quad (46)$$

respectively. From (44) and (45), it follows that $\text{cov}(P, V) = 18(N/4 - |l|)\sigma_s^2\sigma_w^2\alpha^2$.

Appendix B: Approximation for $\Delta = P(0) - P(-1)$

If the estimated l advances one sample from the correct time, $P(l)$ can be rewritten as

$$\begin{aligned} P(-1) \approx & (3N/2 - 7)\sigma_s^2\alpha^2 + \alpha\Re\mathbf{e}[3(W_{12}^H + W_{22}^H\beta^{-1} - W_{32}^H\beta^{-2} + W_{42}^H\beta^{-3})S_1 \\ & - (w_{11}^* + 2w_{21}^*\beta^{-1})s_2], \end{aligned} \quad (47)$$

where W_{i1} and S_2 are replaced by the scalars w_{i1} and s_2 , respectively.

In the absence of timing error, $P(l)$ becomes

$$\begin{aligned} P(0) \approx & 3N\sigma_s^2\alpha^2/2 + 3\alpha\Re\mathbf{e}[(W_{12}^H + W_{22}^H\beta^{-1} - W_{32}^H\beta^{-2} + W_{42}^H\beta^{-3})S_1 \\ & + (w_{21}^* + w_{31}^*\beta^{-1} - w_{41}^*\beta^{-2} + w_5^*\beta^{-3})s_2], \end{aligned} \quad (48)$$

where w_5 is a noise component introduced by the last sample of s_2 . Thus, the difference $P(0) - P(-1)$ can be approximated by

$$P(0) - P(-1) \approx 7\sigma_s^2\alpha^2 + \alpha\Re\mathbf{e}[(w_{11}^* + w_{21}^*(3 + 2\beta^{-1}) + 3w_{31}^*\beta^{-1} - 3w_{41}^*\beta^{-2} + 3w_5^*\beta^{-3})s_2], \quad (49)$$

which can be viewed as a real Gaussian RV with mean $7\sigma_s^2\alpha^2$ and variance $(41 + 12\cos\beta)\sigma_s^2\sigma_w^2\alpha^2$.

Appendix C: Statistical Properties of the Carrier Frequency Offset Estimator

If $l = 0$, $P_1(l)$ can be expressed as

$$\begin{aligned} P_1(0) \approx & 3\alpha^2\beta^{-1}|S|^2 + \alpha\underbrace{(\beta^{-1}W_1^H + \beta^{-2}W_2^H - \beta^{-3}W_3^H)}_{N_1^H}S + \alpha S^H \underbrace{(W_2 - \beta W_3 + \beta^2 W_4)}_{N_2} \\ & + W_1^H W_2 - W_2^H W_3 - W_3^H W_4 \approx 3\alpha^2\beta^{-1}|S|^2 + \alpha(N_1^H S + S^H N_2). \end{aligned} \quad (50)$$

According to (16), the carrier frequency offset estimator is given by

$$\hat{\varepsilon} = \frac{2}{\pi} \arg \left(\frac{\Im[P_1(0)]}{\Re[P_1(0)]} \right) \approx \frac{2}{\pi} \arctan \left(\frac{3\alpha|S|^2 \sin(\varepsilon\pi/2) + \Im(N_1^H S + S^H N_2)}{3\alpha|S|^2 \cos(\varepsilon\pi/2) + \Re(N_1^H S + S^H N_2)} \right). \quad (51)$$

Using the same method as in [2], we can obtain

$$\tan \left[\frac{\pi}{2} (\hat{\varepsilon} - \varepsilon) \right] = \frac{\Im[(P_1(0)\beta]}{\Re[P_1(0)\beta]}. \quad (52)$$

If the estimation error $|\hat{\varepsilon} - \varepsilon|$ is very small, $\tan[\frac{\pi}{2}(\hat{\varepsilon} - \varepsilon)]$ can be approximated by $\frac{\pi}{2}(\hat{\varepsilon} - \varepsilon)$, and (52) becomes

$$\hat{\varepsilon} - \varepsilon \approx \frac{2 \Im[P_1(0)\beta]}{\pi \Re[P_1(0)\beta]} \approx \frac{2}{\pi} \frac{\Im(\beta N_1^H S + \beta S^H N_2)}{3|S|^2 \alpha + \Re(\beta N_1^H S + \beta S^H N_2)} \approx \frac{2}{\pi} \frac{\Im(\beta N_1^H S + \beta S^H N_2)}{3|S|^2 \alpha}, \quad (53)$$

where the last approximation holds at high SNRs. From (53), we infer that the proposed carrier frequency offset estimator is unbiased if there is no timing error. The mean-square error of estimate $\hat{\varepsilon}$ can be obtained after some simple calculations:

$$E[(\hat{\varepsilon} - \varepsilon)^2] = \frac{16}{9 \cdot \pi^2 \cdot N \cdot \text{SNR}}. \quad (54)$$

In the presence of small timing error l , from (40) and (53), it follows

$$\hat{\varepsilon} - \varepsilon \approx \frac{2 \Im(P_1(l)\beta)}{\pi \cdot 3|S_1|^2 \alpha}, \quad (55)$$

where $\Im(P_1(l)\beta)$ is a zero mean RV with variance $N(1 + 10|l|/N)\alpha^2\sigma_w^2/4$ for $|l| < N/4$. In this case, the estimator (51) is still unbiased and its MSE becomes

$$E[(\hat{\varepsilon} - \varepsilon)^2] \approx \frac{16 \cdot (1 + \frac{10|l|}{N})}{9 \cdot \pi^2 \cdot N \cdot \text{SNR} \cdot (1 - \frac{4|l|}{N})^2}. \quad (56)$$

Furthermore, we can extend the above analysis to a more general framework. If a general kind of training symbol (35) with constant length N and frequency offset estimator (36) are assumed, using the same method as in (51)-(53), it is easy to obtain a similar expression for the estimation error

$$\hat{\varepsilon} - \varepsilon \approx \frac{M \Im(\beta' N_1^H S + \beta' S^H N_2)}{2\pi (M-1)|S|^2 \alpha}, \quad (57)$$

where $\beta' := \exp(-j2\pi\varepsilon/M)$, $N_1^H = \sum_{k=1}^{M-1} b_k \exp(j2k\pi\varepsilon/M)W_k^H$ and $N_2 = \sum_{k=2}^M b_k \exp(-j2(k-1)\pi\varepsilon/M)W_k$. Eq. (57) leads to the following general MSE-expression of estimator (36):

$$E[(\hat{\varepsilon} - \varepsilon)^2] = \frac{M^3}{4 \cdot \pi^2 \cdot (M-1)^2 \cdot N \cdot \text{SNR}}. \quad (58)$$

REFERENCES

- [1] R. van Nee and R. Prasad, *OFDM for Wireless Multimedia Communications*, Artech House, 2000.
- [2] P. H. Moose, "A Technique for Orthogonal Frequency Division Multiplexing Frequency Offset Correction," *IEEE Trans. on Commun.*, vol. 42, pp. 2908-2914, Oct. 1994.
- [3] T. M. Schmidl, and D. C. Cox, "Robust frequency and timing synchronization for OFDM," *IEEE Trans. on Commun.*, vol. 45, pp. 1613-1621, Dec.1997.
- [4] S. H. Muller-Weinfurtner, "On the optimality of metrics for coarse frame synchronization in OFDM: A comparison," *Proc. Int. Sym. on Personal, Indoor and Mobile Radio Comm.*, vol. 2, pp. 533-537, Boston, MA, 1998.
- [5] H. Minn, M. Zeng, and V. K. Bhargava, "On timing offset estimation for OFDM systems," *IEEE Communications Letters*, vol. 4, pp. 242-244, July 2000.
- [6] J. J. van de Beek, M. Sandell, and P. O. Borjesson, "ML estimation of time and frequency offset in OFDM systems," *IEEE Trans on Signal Processing*, vol.45, pp.1800-1805, July 1997.
- [7] N. Lashkarian, and S. Kiaei, "Class of Cyclic-Based Estimators for Frequency-Offset Estimation of OFDM Systems," *IEEE Trans. on Commun.*, vol.48, pp.2139-2149, Dec. 2000.
- [8] A. J. Coulson, "Maximum Likelihood Synchronization for OFDM Using a Pilot Symbol: Algorithm," *IEEE Journal on Selected Areas in Commun.*, vol.19, pp.2486-2494, Dec. 2001.
- [9] A. J. Coulson, "Maximum Likelihood Synchronization for OFDM Using a Pilot Symbol: Analysis," *IEEE Journal on Selected Areas in Commun.*, vol.19, pp.2495-2503, Dec. 2001.
- [10] F. Tufvesson, O. Edfors, and M. Faulkner, "Time and frequency synchronization for OFDM using PN-sequence preambles," *Proc. 50th IEEE Vehicular Techn. Conf.*, vol.4, pp. 2203-7, Amsterdam, Netherlands, Sept. 1999.
- [11] E. Sourour and G.E. Bottomley, "Effect of frequency offset on DS-SS acquisition in slowly fading channels," *Proc. IEEE Wireless Commun. and Networking Conf.*, vol.2, pp.569-573, New Orleans, LA, Sept. 1999,
- [12] M. Speth, S. A. Fechtel, G. Fock, and H. Meyr, "Optimum Receiver Design for Wireless Broad-Band Systems Using OFDM-Part I," *IEEE Trans on Commun.*, vol.47, pp.1668-1677, Nov. 1999.
- [13] M. Speth, S. A. Fechtel, G. Fock, and H. Meyr, "Optimum Receiver Design for Wireless Broad-Band Systems Using OFDM-Part II," *IEEE Trans on Commun.*, vol.49, pp.571-578, April. 2001.
- [14] M. Morelli and U. Megali, "An improved frequency offset estimator for OFDM applications", *IEEE Commun. Letters*, vol. 3, pp. 75-77, March 1999.
- [15] M. Morelli and U. Mengali, "Carrier-frequency estimation for transmission over selective channels," *IEEE Transactions on Commun.*, vol. 48, pp. 1580-1589, Sept. 2000.
- [16] J. Li, G. Liu, and G. B. Giannakis, "Carrier frequency offset estimation for OFDM-based WLANs", *IEEE Signal Processing Letters*, vol. 8, pp. 80-82, 2001.
- [17] T. Keller, L. Piazzo, P. Mandarini, and L. Hanzo, "Orthogonal Frequency Division Multiplex Synchronization Techniques for Frequency-Selective Fading Channels," *IEEE Journal on Selected Areas in Commun.*, vol.19, pp.999-1008, June 2001.

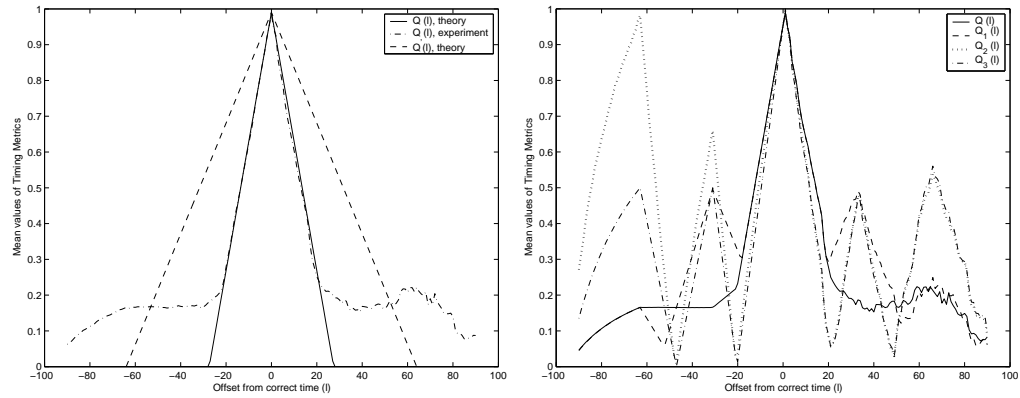


Fig. 1. Mean values of timing metrics for different training symbols, SNR=20dB

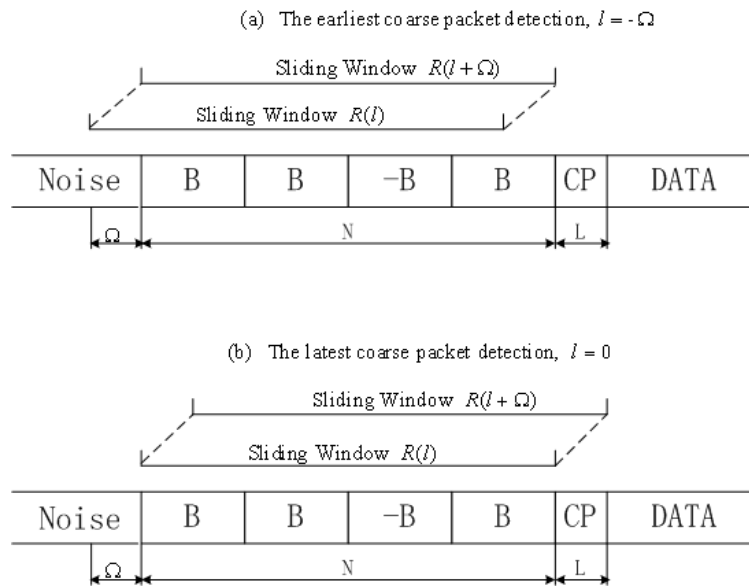


Fig. 2. The relation between l , obtained in the coarse packet detection step, and the sliding windows used in the fine packet detection step ($\Omega = L$)

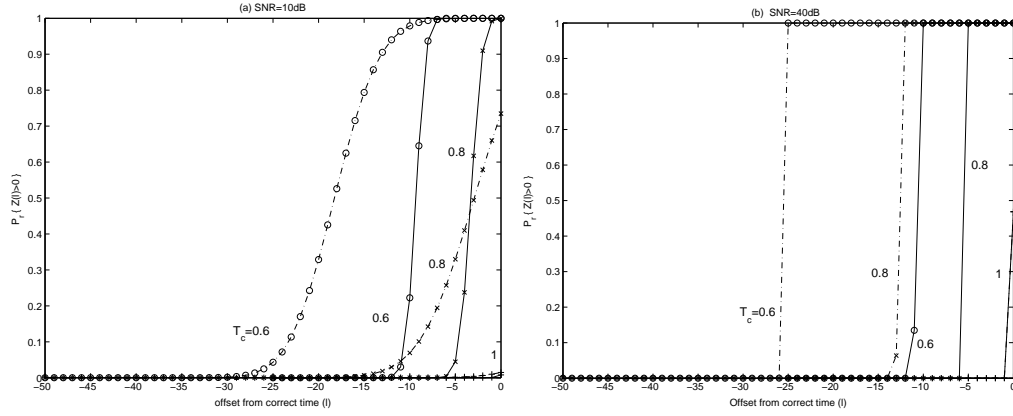


Fig. 3. The probability of $Z(l) > 0$ for (a) $E_s/N_0 = 10\text{dB}$, (b) $E_s/N_0 = 40\text{dB}$. The solid and the dash lines are associated with the metrics corresponding to the training symbols $[+B +B -B +B]$ and $[+A +A]$, respectively. Here we assume $N = 128$ and $L = 16$.

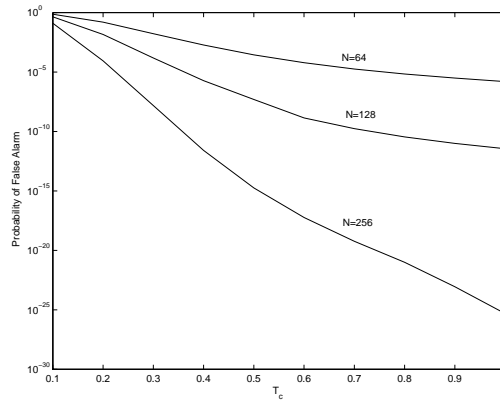


Fig. 4. The Probability of False Alarm versus the Training Symbol Length N and Detection Threshold T_c .

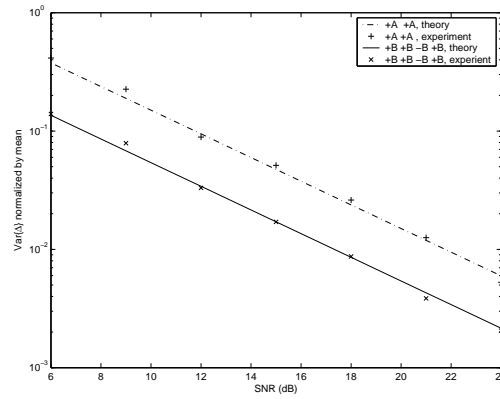


Fig. 5. The Variance of Δ Normalized by Its Mean for the Signaling Set-ups $[+A +A]$ and $[+B +B -B +B]$, $\varepsilon = 0$.

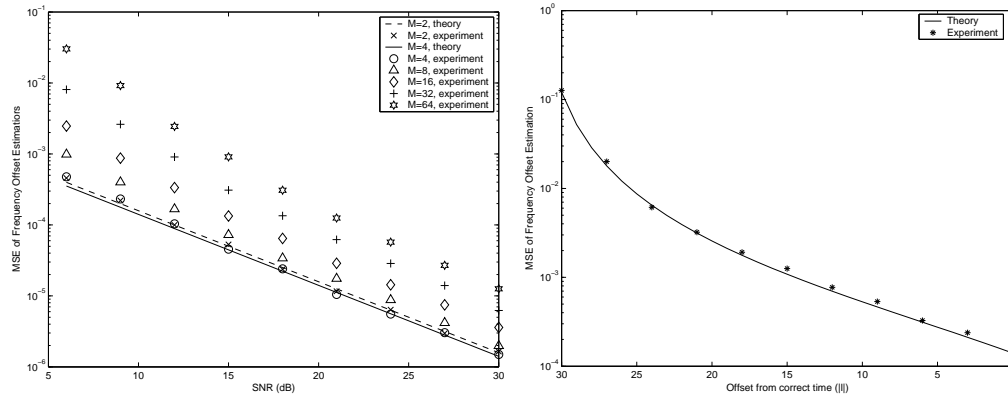


Fig. 6. Mean-Square Error of the Carrier Frequency Offset Estimator in AWGN Channel, $N=128$.

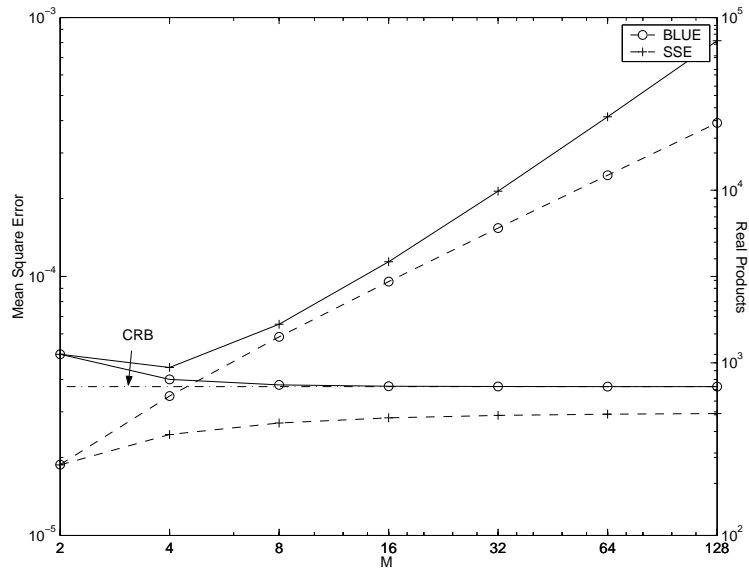


Fig. 7. Comparison of Mean-Square Error (solid line) and Complexity (dash line) of Carrier Frequency Offset Estimators in AWGN Channels, $\text{SNR}=15\text{dB}$, $N=128$.

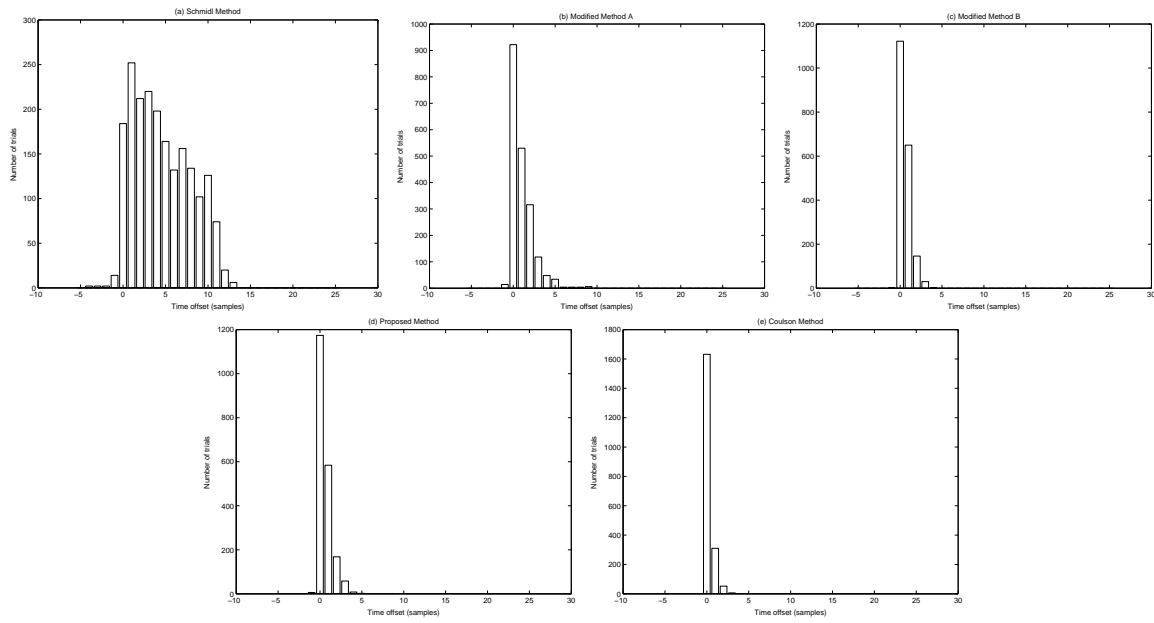


Fig. 8. Time Offset Estimation \hat{l} in Time- and Frequency-Selective Channels

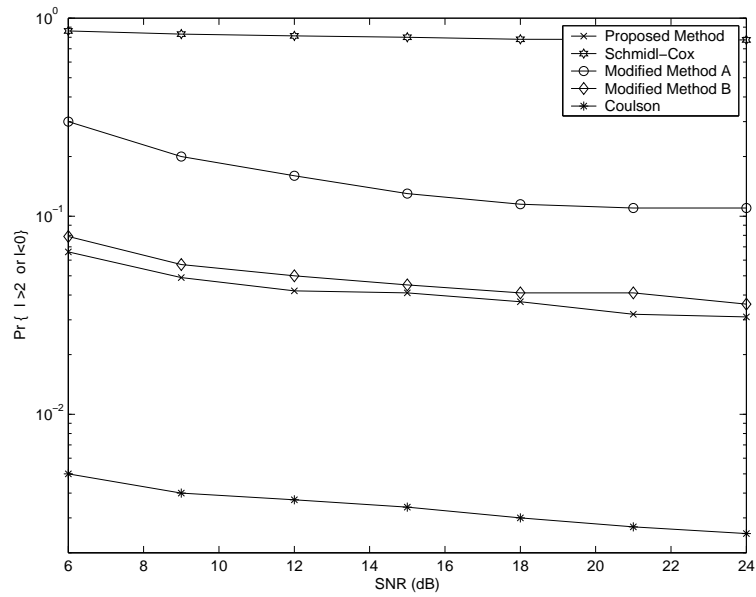


Fig. 9. The Probabilities of Timing Errors that Will Cause ISI in Time- and Frequency-Selective Channels

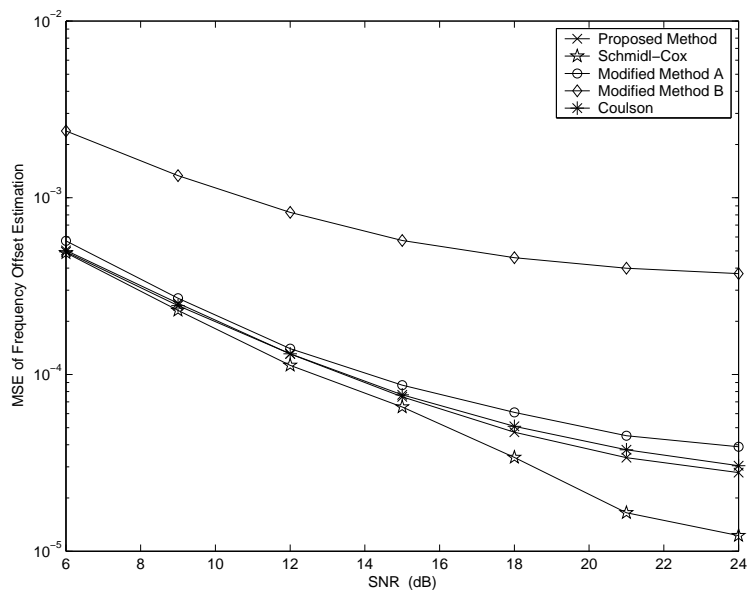


Fig. 10. Mean-Square Error of the Carrier Frequency Offset Estimators in Time- and Frequency-Selective Channels

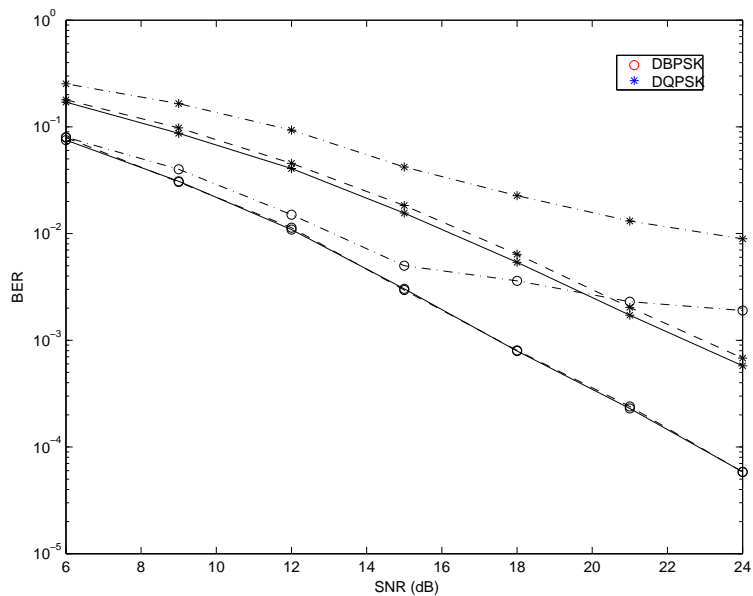


Fig. 11. BER versus SNR in Time- and Frequency-Selective Channels